

StereoScene: BEV-Assisted Stereo Matching Empowers 3D Semantic Scene Completion

Bohan Li^{1,3} Yasheng Sun² Xin Jin^{3†} Wenjun Zeng³

Zheng Zhu⁴ Xiaofeng Wang⁴ Yunpeng Zhang⁴ James Okae⁵ Hang Xiao⁴ Dalong Du⁴

¹Shanghai Jiao Tong University ²Tokyo Institute of Technology

³Eastern Institute for Advanced Study ⁴PhiGent Robotics ⁵South China University of Technology

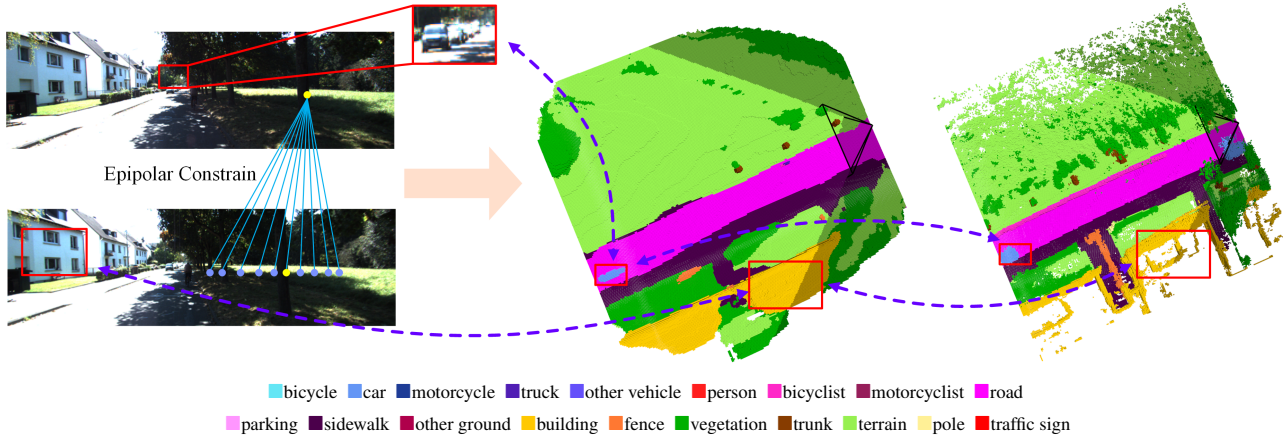


Figure 1: **Overview of StereoScene Framework.** From left to right list stereo input, SSC prediction and ground truth. Our method is able to precisely produce semantic scenery and capture small distant objects (see the car marked by red box).

Abstract

3D semantic scene completion (SSC) is an ill-posed task that requires inferring a dense 3D scene from incomplete observations. Previous methods either explicitly incorporate 3D geometric input or rely on learnt 3D prior behind monocular RGB images. However, 3D sensors such as LiDAR are expensive and intrusive while monocular cameras face challenges in modeling precise geometry due to the inherent ambiguity. In this work, we propose **StereoScene** for 3D Semantic Scene Completion (SSC), which explores taking full advantage of light-weight camera inputs without resorting to any external 3D sensors. Our key insight is to leverage stereo matching to resolve geometric ambiguity. To improve its robustness in unmatched areas, we introduce bird’s-eye-view (BEV) representation to inspire hallucination ability with rich context information. On top of the stereo and BEV representations, a mutual interactive aggregation (MIA) module is carefully devised to fully unleash their power. Specifically, a Bi-directional Interaction Transformer (BIT) augmented with confidence reweighting is used to encourage reliable prediction through

mutual guidance while a Dual Volume Aggregation (DVA) module is designed to facilitate complementary aggregation. Experimental results on SemanticKITTI demonstrate that the proposed StereoScene outperforms the state-of-the-art camera-based methods by a large margin with a relative improvement of 26.9% in **geometry** and 38.6% in **semantic**. Our code is available on <https://github.com/Arlo0o/StereoScene>.

1. Introduction

3D scene understanding is a fundamental task in computer vision [44], facilitating a variety of applications such as autonomous driving, robotic navigation and augmented reality. Due to the limitations of real-world sensors such as restricted field of view, measurement noise, or sparse results, this task remains a challenging problem. To address this problem, 3D Semantic Scene Completion (SSC) [47] is introduced to jointly predict the geometry and semantic segmentation of a scene. Given its inherent 3D nature, most existing SSC solutions [17, 46, 58] employ 3D geometric signals, in the form of occupancy grids, point clouds, or distance fields, as their model inputs. Although they provide

[†]Corresponding author, jinxin@eias.ac.cn

insightful geometric cues, it requires costly sensors (e.g. LiDAR) alongside considerable manual labor entailed in their deployment. Hence, it is worth exploring an efficient and effective approach for high-fidelity SSC solely with portable cameras.

However, lifting 2D image features to 3D is a notoriously ill-posed task due to its inherent uncertainty of incomplete observation and scale ambiguity at single viewpoint [16]. Previous camera-based SSC solutions [4] attempt to tackle this challenge by converting 2D image features to 3D dense space with a 2D-3D projection UNet. Solely relying on 3D prior without geometric constraint, the predicted voxel occupancy inevitably falls short of capturing accurate geometric features.

In this paper, we propose **StereoScene**, a framework that targets to fully exploit the potential of vision inputs with stereo matching as Figure 1. With explicit geometric constraint, stereo matching exhibits exceptional proficiency in producing precise predictions on matched positions. However, stereo matching is sensitive to calibration settings and susceptible to failure in challenging circumstances such as high-reflectance illumination or occluded regions, since it heavily relies on feature correspondence between camera rigs. By contrast, BEV based approaches implicitly convert image features to a canonical space independent of camera setups. Given that this latent representation is directly induced from image features, it encodes rich context and semantic information, demonstrating strong global robustness and hallucination capability [29]. Based on the above observation, our primary objective is to *devise an integration mechanism to dynamically incorporate dependable BEV predictions without compromising the stereo construction results*.

To this end, we thus propose a BEV-assisted stereo matching SSC framework to make the best of both representations: **1)** After carefully examining the BEV and stereo construction procedure, we identify that stereo geometric volume and BEV latent volume are suitable for effective mutual reinforcement. **2)** Given these two volumes withholding distinct natures, we devise a *Mutual Interactive Aggregation Module* that follows bootstrap-before-fuse paradigm. Particularly, A *Bi-directional Interaction Transformer (BIT)* is designed to guide each other to screen reliable information, on top of which a confidence re-weighting strategy inspired by MVS [9] is introduced to further enhance the boost performance. Besides, a *Dual Volume Aggregation Module* is delicately designed to facilitate complementary aggregation.

Our contributions are summarized as follows: **1)** We propose a BEV-assisted stereo matching framework for 3D semantic scene completion. **2)** To bridge the representation gap, a Transformer-based *Mutual Interactive Aggregation Module* is designed for combining their comple-

mentary merits. **3)** Extensive experiments demonstrate that our StereoScene approach outperforms all the camera-based state-of-the-arts by a large margin, with a relative improvement of 26.9% in **geometry** and 38.6% in **semantic** on SemanticKITT.

2. Related Works

2.1. Semantic Scene Completion

Earlier works on scene completion (SC) used sophisticated interpolation [13] or energy minimization [23, 34, 51] techniques to estimate 3D dense geometry given one or more 2D/3D observations. With the large-scale datasets [2, 49, 50, 52] released in recent years, recent works [3, 43, 59, 11, 50, 58, 46, 25] have increasingly relied on deep learning techniques to learn 3D priors and address ambiguity in the scene. Song et al. [50] recognized the intertwined relationship between semantic segmentation and scene completion and proposed a joint estimation of semantic segmentation and scene completion.

Given the 3D nature of semantic scene completion task, many studies [61, 43, 17, 58] directly use 3D inputs to take advantage of its accompanying geometrical insights. To provide additional texture or geometry information, a vast majority of works [3, 26, 15, 25, 12] exploit multi-modal inputs, such as RGB images coupled with various geometric cues. IPF-SPCNet [62] performs semantic segmentation on the image inputs and uses RGB features to augment the 3D point cloud. Another slew of studies [4, 28] aim to achieve semantic scene completion solely with camera-only vision inputs. For instance, MonoScene [4] lifts a monocular image using 2D-3D projections and leverages 2D and 3D UNets for semantic scene completion. VoxFormer [28] takes multiple temporal images as inputs and employs a transformer-based framework where a sparse set of visible and occupied voxel queries are devised for reliable scene structure reconstruction. Another work that also attempts to exploit geometry constraint by vision inputs is OccDepth [33]. However, they rely on a pre-trained depth network for 3D knowledge distillation in the training process, causing heavy computation overhead.

2.2. Stereo Matching Based 3D Perception

With the advances of deep convolutional neural networks, the quality of depth predicted from stereo images [41] has steadily improved and has led to a remarkable improvement in downstream 3D vision applications such as object detection, surface reconstruction and semantic scene completion. GC-Net [24] was the first to propose 3D CNNs based stereo depth prediction framework, where potential stereo corresponding 2D features are mapped to a 3D cost volume through a concatenation operation. The promise of this method inspired GwcNet [19], which pro-

poses group-wise correlation to improve feature similarity measurement. Recent state-of-the-art stereo matching methods can be broadly categorized into 2D CNN based approaches [32, 38, 20, 54] and 3D CNN based approaches [24, 5, 19, 36]. More recent 2D CNN methods such as RAFT-Stereo [14] and CREStereo [27] utilize correlation to produce matching cost volume which is subsequently optimized through sequential refinement modules for depth prediction. However, in conditions such as occlusion and large textureless regions, stereo depth prediction performance drops significantly.

2.3. Bird’s-eye-View Representation

The bird’s-eye-view is a widely used representation of a surrounding scene since it provides a clear depiction of the layout and shape of objects from a top-down perspective. Due to its effectiveness on dense representations, BEV has been broadly employed to map segmentation approaches [40, 21, 35, 37, 31, 45], benefiting perception and motion planning in autonomous driving scenarios. In camera-based scene understanding frameworks, researchers lift 2D image features to 3D BEV representations coupled with estimated depth distribution [42, 40, 29]. Mani et.al. [31] utilize a ResNet to reason about bird’s-eye-view layout, whereas Roddick et.al. [45] devise a transformer architecture to predict map semantic segmentation with converted BEV representations. Lift-Splat [40] extracts BEV representations from an arbitrary number of cameras by implicitly unprojecting 2D visual inputs based on estimated depth distribution. To circumvent compounding errors [57], later approaches attempt to dynamically learn reliable geometric insights rather than relying on structural 3D prior. BEVFormer [29] design a spatial-temporal transformer to adaptively extract and aggregate BEV features from images at different timestamps. However, current BEV approaches still struggle to capture accurate geometric information in complicated scenarios due to the absence of explicit geometric constraints. In this work, we seek to explore more reliable geometric cues by exploiting stereo geometric cues and BEV semantic representations. We demonstrate that this idea provides more reliable geometric cues for improved semantic scene completion performance.

3. Methodology

We present our **StereoScene** framework that aims to jointly infer dense 3D geometry and semantics from solely camera-based stereo RGB images. The whole pipeline is depicted in Figure 2. In this section, we first explore a hybrid occupancy based SSC learning formulation (Sec. 3.1), then we provide detailed construction of *dual volume* representation (Sec. 3.2). To bridge their representation gap, we depict our devised aggregation module (Sec. 3.3). Finally, we introduce our SSC generator and training paradigm

(Sec. 3.4).

3.1. Preliminary

Problem Formulation. Given a set of stereo RGB images $I_{Stereo}^{rgb} = \{I_l^{rgb}, I_r^{rgb}\}$, our goal is to jointly infer geometry and semantics of a 3D scene. The scene is represented as a voxel grid $\mathbf{Y} \in \mathbb{R}^{H \times W \times Z}$, where H, W, Z denote the height, width and depth in 3D space. Regarding each voxel, it will be assigned to a unique semantic label belonging to $C \in \{c_0, c_1, \dots, c_M\}$, which either occupies empty space c_0 or falls on a specific semantic class $\{c_1, c_2, \dots, c_M\}$. Here M denotes the total number of semantic classes. We would like to learn a transformation $\hat{\mathbf{Y}} = \Theta(I_{Stereo}^{rgb})$ to approach ground truth 3D semantics \mathbf{Y} .

Architecture Overview. The overall architecture of our StereoScene framework is illustrated in Figure 2. We follow common paradigm [4] that employs successive 2D and 3D UNets as backbones. The input stereo images I_{Stereo}^{rgb} are separately encoded by a 2D UNet into paired context-aware features \mathbf{F}_l and $\mathbf{F}_r \in \mathbb{R}^{C \times H \times W}$. Then we leverage a *Stereo Constructor* to convert these features into a dense 3D volume $\mathbf{V}_{Stereo} \in \mathbb{R}^{D_s \times H \times W}$. In parallel, a *BEV Constructor* lift 2D features \mathbf{F}_l of left image to a latent BEV volume $\mathbf{V}_{BEV} \in \mathbb{R}^{D_b \times H \times W}$ alongside its context feature $\mathbf{C}_{BEV} \in \mathbb{R}^{C_b \times H \times W}$ following standard protocol of [40]. Sequentially, the two-stream built volumes are bridged and aggregated to a new volume \mathbf{V}_{agg} by a *Mutual Interactive Aggregation Module*. Finally, the context feature \mathbf{C}_{BEV} splat along volume \mathbf{V}_{agg} by outer-product, which will be fed to a 3D UNet for semantic segmentation and completion.

3.2. Dual Volume Construction

Unlike previous studies [17, 46, 58], we aim to resolve holistic 3D scene understanding without resorting to any 3D geometric inputs. To encode 2D image features to 3D space, we introduce a hybrid volume representation, stereo volume and BEV volume, withholding two distinct natures to take full advantage of camera inputs.

Shared 2D Feature Extraction Backbone. For the purpose of image feature extraction, 2D UNet with pre-trained EfficientNetB7 [53] is leveraged to separately process left and right input images. Note that we utilize shared weights to encourage efficient context learning in canonical space.

Stereo Geometric Volume Constructor. With the obtained unary features \mathbf{F}_l and \mathbf{F}_r from left and right images, *Stereo Constructor* targets to build a voxel depth volume \mathbf{V}_{Stereo} by matching them with epipolar constraint. Specially, group-wise correlation [19] is adopted to generate disparity cost volume. Formally,

$$D_{gwc}(d, x, y, g) = \frac{1}{N_c/N_g} \langle f_g^l(x, y), f_g^r(x - d, y) \rangle, \quad (1)$$

where $\langle \cdot, \cdot \rangle$ represents the inner product, N_c is the channels

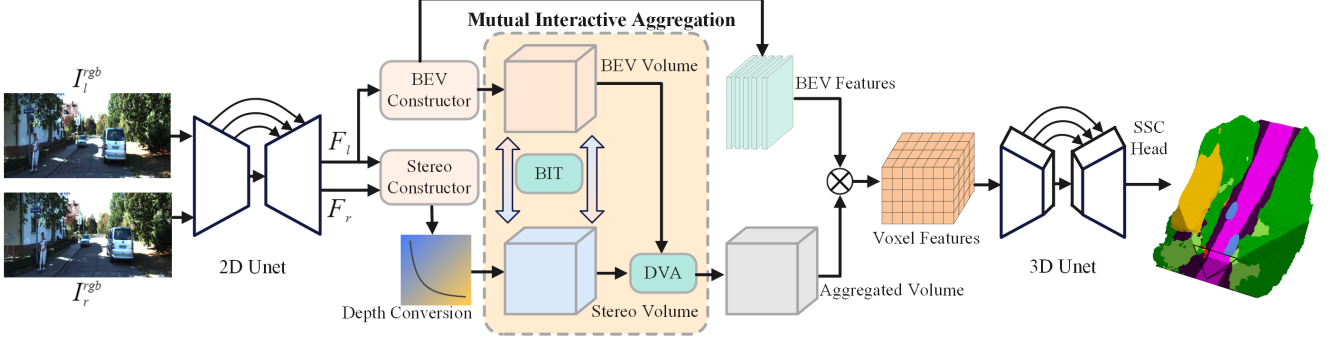


Figure 2: Overall framework of our proposed **StereoScene**. Given input stereo images, we employ 2D UNet to extract multi-scale features. The BEV latent volume and stereo geometric volume are constructed by a *BEV Constructor* and a *Stereo Constructor*, respectively. To fully exploit the complementary potential of the two volumes, a *Mutual Interactive Aggregation Module* is proposed to mutually bootstrap and aggregate them.

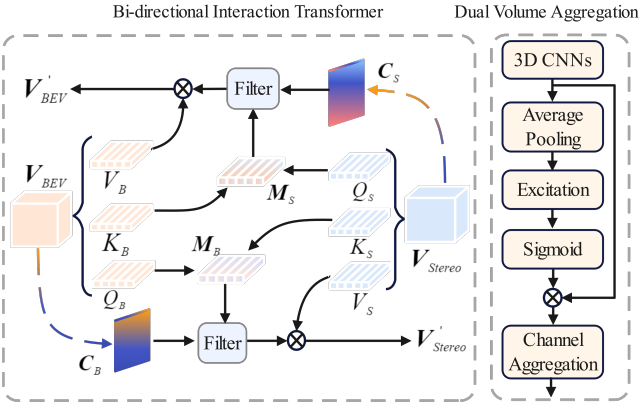


Figure 3: The structure of proposed *Mutual Interactive Aggregation* module. We employ *Bi-directional Interactive Transformer* for reliable geometry information interaction. Afterwards, the interacted volumes are concatenated together and fed into *Dual Volume Aggregation* module to generate the aggregated volume.

of input features, N_g is the number of groups, f_g^l and f_g^r represent g^{th} left and right feature group, respectively. Afterwards, the disparity volume is converted into a depth volume following [60], which is formulated as:

$$z_{(u,v)} = \frac{f_u \times b}{D_{(u,v)}}, x = \frac{(u - c_u) \times z}{f_u}, y = \frac{(v - c_v) \times z}{f_v}, \quad (2)$$

where f_u and f_v represent the horizontal and vertical focal length, (c_u, c_v) is the camera center. So far, the dense stereo volume \mathbf{V}_{Stereo} involving spatial depth is constructed.

BEV Latent Volume Constructor. Although stereo constructor provides accurate estimation in aligned locations, it struggles in extreme conditions where severe occlusion or high reflection happens. Unlike stereo-based approach relying on strict geometric matching, BEV representations are obtained by lifting an image I^{rgb} to a shared bird’s eye

space through 3D prior. Following [40], we feed visual features \mathbf{F}_l to a convolution neural network and obtain a latent depth distribution $\mathbf{V}_{BEV} \in \mathbb{R}^{D_b \times H \times W}$ with its associated context features $\mathbf{C}_{BEV} \in \mathbb{R}^{C_b \times H \times W}$. Since this distribution is essentially a voxel grid that stores the probability of all possible depths, we denote it as BEV latent volume for the sake of clarity.

3.3. Mutual Interactive Aggregation Module

With the obtained stereo volume \mathbf{V}_{Stereo} and BEV volume \mathbf{V}_{BEV} , this module aims to mutually reinforce each other and integrate their respective potentials to produce a new volume \mathbf{V}_{agg} .

Bi-directional Interactive Transformer. For superior aggregation, we propose an initial bootstrapping stage that selectively screens dependable information alongside its counterpart volume. Concretely, a Bi-directional Interactive Transformer (BIT) as Figure 3 is devised to interactively guide reliable predictions of its contrary side through cross-attention mechanism. For stereo volume \mathbf{V}_{Stereo} , we first obtain its query Q_S , key K_S and value V_S following standard protocol [55, 56]. Similarly, the BEV volume \mathbf{V}_{BEV} is forwarded and its query, key and value are denoted as Q_B, K_B, V_B , respectively. Then we construct a guidance attention matrix $\mathbf{M}_S \in \mathbb{R}^{HW \times HW}$ indicating the interactive guidance, which is implemented by a cross-attention operation as:

$$\mathbf{M}_S = CrossAtt(\mathbf{V}_{Stereo}, \mathbf{V}_{BEV}) = softmax(K_B^T Q_S), \quad (3)$$

In this way, \mathbf{M}_S accounts for the relevant aspects of the stereo sides, thereby providing an alternative perspective on spatial importance of the BEV side. Likewise, \mathbf{M}_B is computed by $softmax(K_S^T Q_B)$ to encourage reliable geometry information transmission.

Depth Confidence Filtering. In order to further enhance the guidance matrix described above, we develop a depth confidence filtering strategy, which explicitly takes advan-

tage of the involved geometry information behind the volume. We aim to utilize its depth distribution information to enforce the guidance matrix similar to [9]. Particularly, to project the volume to a confidence map $\mathbf{C}_S \in \mathbb{R}^{H \times W}$, we first adopt *softmax* to convert depth cost value d_i into probability form, and then take out the highest probability value among all depth hypothesis planes along the depth dimension as the prediction confidence. The process is formally written as:

$$\mathbf{C}_S = WTA \left\{ \frac{\exp(d_i)}{\sum_{j=1}^{D_{max}} \exp(d_j)} \right\}, \quad (4)$$

where the *softmax* is applied across the depth dimension and *WTA* represents winner-takes-all operation. D_{max} denotes the length of depth dimension. To this end, we update the previous attention matrix with reshaped confidence map $\mathbf{C}_S \in \mathbb{R}^{1 \times HW}$ as follows:

$$\mathbf{M}'_S = \mathbf{M}_S \odot \mathbf{C}_S, \quad (5)$$

where \odot represents element-wise multiplication, through which the geometry information of reliable areas is preserved while low-confidence areas are suppressed.

Finally, the filtered inter-attention matrix \mathbf{M}'_S is leveraged to multiply the BEV value vector V_B to obtain the interacted BEV volume \mathbf{V}'_{BEV} .

$$\mathbf{V}'_{BEV} = \mathbf{M}'_S \odot V_B, \quad (6)$$

Note that its opposite interacted volume \mathbf{V}'_{Stereo} is calculated in a symmetric manner.

Dual Volume Aggregation. With the bootstrapped volume representations \mathbf{V}'_{Stereo} and \mathbf{V}'_{BEV} , the primary objective of this module is to leverage their strengths and facilitate a mutually beneficial complementation and aggregation. Specially, the volume aggregation module takes as input concatenated features $\mathbf{V}'_{cat} = [\mathbf{V}'_{Stereo}, \mathbf{V}'_{BEV}] \in \mathbb{R}^{2 \times D \times H \times W}$ and outputs aggregated volume \mathbf{V}_{agg} . As illustrated in Figure 3, the input is first fed into residual 3D CNNs for regularization and channel adjustment, which generates transformed representation $\mathbf{V}_f \in \mathbb{R}^{C \times D \times H \times W}$. To fully exploit its contextual information [22], we utilize average pooling to squeeze the information into a channel descriptor $\mathbf{z}_c \in \mathbb{R}^C$. We shrink \mathbf{V}_f along both the depth dimension D and spatial dimension $H \times W$,

$$\mathbf{z}_c = \frac{1}{D \times H \times W} \sum_{d=1}^D \sum_{i=1, j=1}^{H, W} \mathbf{V}_f(d, i, j), \quad (7)$$

Subsequently, an excitation block [22] is leveraged to capture its channel-wise dependencies. Formally, the channel descriptor is updated to \mathbf{z}'_c by two stacked bottleneck-convolutions with non-linear activation as:

$$\mathbf{z}'_c = \sigma(\mathbf{W}_2 \delta(\mathbf{W}_1 \mathbf{z}_c)), \quad (8)$$

where the W_1 and W_2 represent $1 \times 1 \times 1$ convolutions with dimensionality-reduction. The δ denotes standard GELU and the σ indicates sigmoid gate. Then \mathbf{z}'_c is employed to re-weight the previous transformed feature \mathbf{V}_f along the channel dimension. After re-weighting, we aggregate information between different channels. Formally,

$$\mathbf{V}_{agg} = \mathbb{P}(\mathbf{z}'_c \odot \mathbf{V}_f), \quad (9)$$

where \mathbb{P} is composed of point-wise convolution with GELU activation and group normalization. The point-wise convolution encourages channel-aware mixing by $1 \times 1 \times 1$ kernel size, through which the aggregated volume \mathbf{V}_{agg} takes into consideration features of different aspects.

3.4. Semantic Scene Completion

To make use of this high-quality occupancy grid \mathbf{V}_{agg} for semantic scene completion, we augment it with its associated context information \mathbf{C}_{BEV} . The extracted context information from input images is placed to a specific location of the bird-eye’s representation by an outer product operation similar to [40]. Formally, the aggregated 3D feature $\mathbf{F}_{agg} \in \mathbb{R}^{C_b \times D_b \times H \times W}$ is computed by:

$$\mathbf{F}_{agg} = \mathbf{C}_{BEV} \otimes \mathbf{V}_{agg}, \quad (10)$$

where the \mathbf{V}_{agg} and \mathbf{C}_{BEV} is firstly unsqueezed on channel dimension and depth dimension, respectively. In this way, we are able to seamlessly blend the complementary benefits of stereo representation for precise geometry and BEV features for rich semantic context.

Semantic Segmentation Learning. Following [4], we leverage an encoder-decoder 3D UNet to process the aggregated 3D voxel features. Its output features are fed to a SSC head for semantic occupancy prediction $\hat{\mathbf{Y}}$. The SSC head is composed of a 3D ASPP [6] block and a softmax layer.

Network Training. We follow the basic learning objective of MonoScene [4] for semantic scene completion. Standard semantic loss \mathcal{L}_{sem} and geometry loss \mathcal{L}_{geo} are leveraged for semantic and geometry supervision, while an extra class weighting loss \mathcal{L}_{ce} is also added as [4]. To further enforce the aggregated volume \mathbf{V}_{agg} , we adopt a binary cross entropy loss \mathcal{L}_{depth} to encourage the sparse depth distribution. The overall learning objective of this framework is formulated as follows:

$$\mathcal{L} = \mathcal{L}_{depth} + \lambda_{ce} \mathcal{L}_{ce} + \lambda_{sem} \mathcal{L}_{sem} + \lambda_{geo} \mathcal{L}_{geo}. \quad (11)$$

where λ s are balancing coefficients.

4. Experiments

4.1. Experimental Settings

Datasets. We evaluate the proposed StereoScene on SemanticKITTI [2] that is popularly used in a great number of

Methods	StereoScene (ours)	MonoScene [4]	JS3CNet [59]	LMSCNet [46]	AICNet [25]	3DSketch [10]
IoU (%)	43.34	34.16	34.00	31.38	23.93	26.85
mIoU	15.36	11.08	8.97	7.07	7.09	6.23
■ car (3.92%)	22.8	18.80	<u>20.10</u>	14.30	15.30	17.10
■ bicycle (0.03%)	3.40	0.50	0.00	0.00	0.00	0.00
■ motorcycle (0.03%)	2.40	0.70	0.00	0.00	0.00	0.00
■ truck (0.16%)	<u>2.80</u>	3.30	0.80	0.30	0.70	0.00
■ other-veh. (0.20%)	6.10	<u>4.40</u>	4.10	0.00	0.00	0.00
■ person (0.07%)	2.90	<u>1.00</u>	0.00	0.00	0.00	0.00
■ bicyclist (0.07%)	2.20	<u>1.40</u>	0.20	0.00	0.00	0.00
■ motorcyclist (0.05%)	0.50	<u>0.40</u>	0.20	0.00	0.00	0.00
■ road (15.30%)	61.90	<u>54.70</u>	47.30	46.70	39.30	37.70
■ parking (1.12%)	30.70	<u>24.80</u>	19.90	13.50	19.80	0.00
■ sidewalk (11.13%)	31.20	<u>27.10</u>	21.70	19.50	18.30	19.80
■ other-grnd (0.56%)	10.70	<u>5.70</u>	2.80	3.10	1.60	0.00
■ building (14.10%)	24.20	<u>14.40</u>	12.70	10.30	9.60	12.10
■ fence (3.90%)	16.50	<u>11.10</u>	8.70	5.40	5.00	3.40
■ vegetation (39.3%)	23.80	<u>14.90</u>	14.20	10.80	9.60	12.10
■ trunk (0.51%)	8.40	2.40	<u>3.10</u>	0.00	1.90	0.00
■ terrain (9.17%)	27.00	<u>19.50</u>	12.40	10.40	13.50	16.10
■ pole (0.29%)	7.00	<u>3.30</u>	1.90	0.00	0.10	0.00
■ traf.-sign (0.08%)	7.20	<u>2.10</u>	0.30	0.00	0.00	0.00

Table 1: **Quantitative results** on the SemanticKITTI hidden test set with the state-of-the-art **camera-based** SSC methods. The top two performers are marked **bold** and underlined, respectively.

Methods	Input	IoU(%) \uparrow	mIoU(%) \uparrow
StereoScene (ours)	Stereo	<u>43.85</u>	15.43
MonoScene [4]	Mono	36.80	11.30
Voxformer-T [28]	Stereo	44.15	<u>13.35</u>
LMSCNet [46]	Mono	38.36	9.94
SSCNet [50]	Mono	40.93	10.27

Table 2: **Quantitative results** on the SemanticKITTI validation set against the state-of-the-art camera-based SSC methods. Voxformer-T adopts multiple temporal stereo images as inputs.

previous studies. There are 22 driving outdoor scenes from the KITTI Odometry Benchmark [18], covering diverse and challenging autonomous driving situations. SemanticKITTI holds semantic annotations of LiDAR sweeps that are registered, aggregated and voxelized as $256 \times 256 \times 32$ grid of 0.2m voxels. The target ground truth of each voxel grid is annotated as one of 21 classes (1 unknown, 1 free and 19 semantics). The SemanticKITTI benchmark provides both voxelized LiDAR scans and RGB images as model input options. We solely utilize RGB images since our main focus is to explore the portable camera-only signals as MonoScene [4].

Implementation Details. We set the 3D UNet input to $128 \times 128 \times 16$ (1:2) for efficient memory usage, whose fea-

ture will be upscaled to 1:1 at completion head by deconvolution operation. The λ s are empirically set to 1. Our models are implemented on PyTorch [39] with two Tesla A100 GPUs. We train 30 epochs employing an AdamW [30] optimizer with a learning rate of $1e-4$ and batch size set to 10.

Comparison Methods. We compare our method with the best models [28, 4, 59, 46, 25, 10] currently available that support 3D semantic scene completion(SSC). **MonoScene** [4] is a very-first camera-based SSC method, relying on feature projection for 2D-to-3D scene reconstruction. **VoxFormer-T** [28] is the temporary version of VoxForme-S that leverages a sequential of stereo images. Other baselines such as **JS3CNet** [59], **LMSCNet** [46], **SSCNet** [50], **AICNet** [25] and **3DSketch** [10] require 3D geometric input. For fair comparison, we adapt these baselines with pseudo 3D inputs inferred from images following similar protocols as previous methods [28, 4].

Evaluation Metrics. Regarding quantitative evaluations, we conduct experiments on metrics [28, 4] that have been widely employed in the field of SSC. We leverage **IoU** (Intersection over Union) to account for SC task and **mIoU** (mean Intersection over Union) to measure the performance of SSC task, respectively. For both of these two metrics, higher values are desirable, where high IoU indicates accurate geometric prediction and high mIoU implies precise semantic segmentation.

4.2. Performance

Quantitative Comparison. Table 1 reports the performance of our StereoScene and other camera-based baselines on the SemanticKITTI hidden test set. Our approach outperforms MonoScene by a large margin in terms of geometric completion and semantic segmentation. Significantly, the IoU is improved by 26.9% (34.16%→43.34%) while the mIoU is improved by 38.6% (11.08%→15.36%). Except for the truck category (0.5 lower than MonoScene), StereoScene has surpassed other baselines in terms of individual category prediction.

It’s worth noting that our method demonstrates significant superiority in the prediction of small moving objects compared to MonoScene, including bicycle (0.50%→3.40%), motorcycle (0.70%→2.40%), person (1.00%→2.90%), trunk (2.40%→8.40%), pole (3.30%→7.00%), etc. We ascribe such improvements to the introduction of dual volume, which is critical for 3D geometry awareness.

As shown in Table 2, we also report the quantitative results on the SemanticKITTI validation set. Although Voxformer-T employs up to 4 temporal stereo image pairs as inputs, our method has only a negligible difference in IoU but a significant advantage in mIoU, with a 36.5% improvement over MonoScene and a 15.6% improvement over Voxformer-T.

Qualitative Comparison. As shown in Figure 4, we compare the visualization results of our StereoScene and MonoScene on the SemanticKITTI validation set. Due to the complexity of the outdoor scenes and the sparsity of the labels, it is challenging to reconstruct the geometry of the scenes accurately and completely. Compared to MonoScene, our StereoScene evidently captures better geometric representations to reconstruct more complete scenes with correct classes (e.g. vegetation and terrain beside the road). It is worth noting that our StereoScene can generate accurate 3D scene layout even in cluttered scenarios, which is attributed to explicit geometry awareness. For example, in the second column, StereoScene not only reconstructs the scene on the right side of the road, but also distinguishes the sidewalk more properly compared to MonoScene.

Our method shows obvious advancement on small moving objects compared to MonoScene (e.g. cars in column 1 and column 4). Moreover, for regions outside the camera’s field of view (voxels in darker regions), StereoScene is capable of hallucinating a more reasonable and complete scene compared to MonoScene (e.g. darker regions in column 1, column3).

4.3. Ablation Study

We ablate our StereoScene on the SemanticKITTI validation set for scene completion and semantic scene completion. For both tasks, we use only RGB images as inputs.

Architecture Components	IoU(%)↑	mIoU(%)↑
Ours	42.85	15.29
Ours w/o Depth Conversion	41.94	15.12
Ours w/o BiT Module	41.60	14.19
Ours w/o DVA Module	42.28	15.16

Table 3: Ablation study for architecture components.

Feature Scales				IoU (%)↑	mIoU (%)↑
$\frac{1}{32}$	$\frac{1}{16}$	$\frac{1}{8}$	$\frac{1}{4}$		
✓				40.08	13.40
✓	✓			41.28	14.29
✓	✓	✓		42.68	14.93
✓	✓	✓	✓	42.85	15.29

Table 4: Ablation study for feature scales. Feature scales are related to the resolution of the input image.

Volumes	IoU(%)↑	mIoU(%)↑
Ours	42.85	15.29
Ours w/o Stereo Volume	38.97	13.18
Ours w/o BEV Volume	41.71	13.71
Ours w/o Confidence Filtering	42.19	14.67

Table 5: Ablation study for the dual volume. The best performance is achieved by aggregating the both volumes with confidence filtering.

Effect of Architecture Components. We conduct architectural ablation to evaluate the impact of different components of our network as shown in Table 3. The BIT module can significantly improve the geometric and semantic estimations (+1.25 IoU, +1.10 mIoU). Compared with the DVA module, the depth conversion can boost geometric prediction by a relatively larger margin (+0.91 IoU), while having less impact on semantic prediction (+0.17 mIoU).

Effect of 2D Feature Scales. The ablation study for the 2D image feature scales is shown in Table 4. We construct image features with different scales by adjusting the convolution strides in the 2D UNet. As we can see from the table, the results can be significantly improved by combining features with different scales, increasing the IoU from 40.08 to 42.85 and mIoU from 13.40 to 15.29, respectively.

Effect of Dual Volume. The ablation study for the dual volume is shown in Table 4. We first build the framework pipeline with an individual volume and maintain the DVA module to verify the effect. We find that after removing the stereo volume, the geometric perception ability of the framework decreases dramatically (-3.88 IoU), while the prediction performance of semantic scene segmentation is affected as well (-2.11 mIoU). The introduction of BEV volume has a relatively greater impact on the semantic aspect

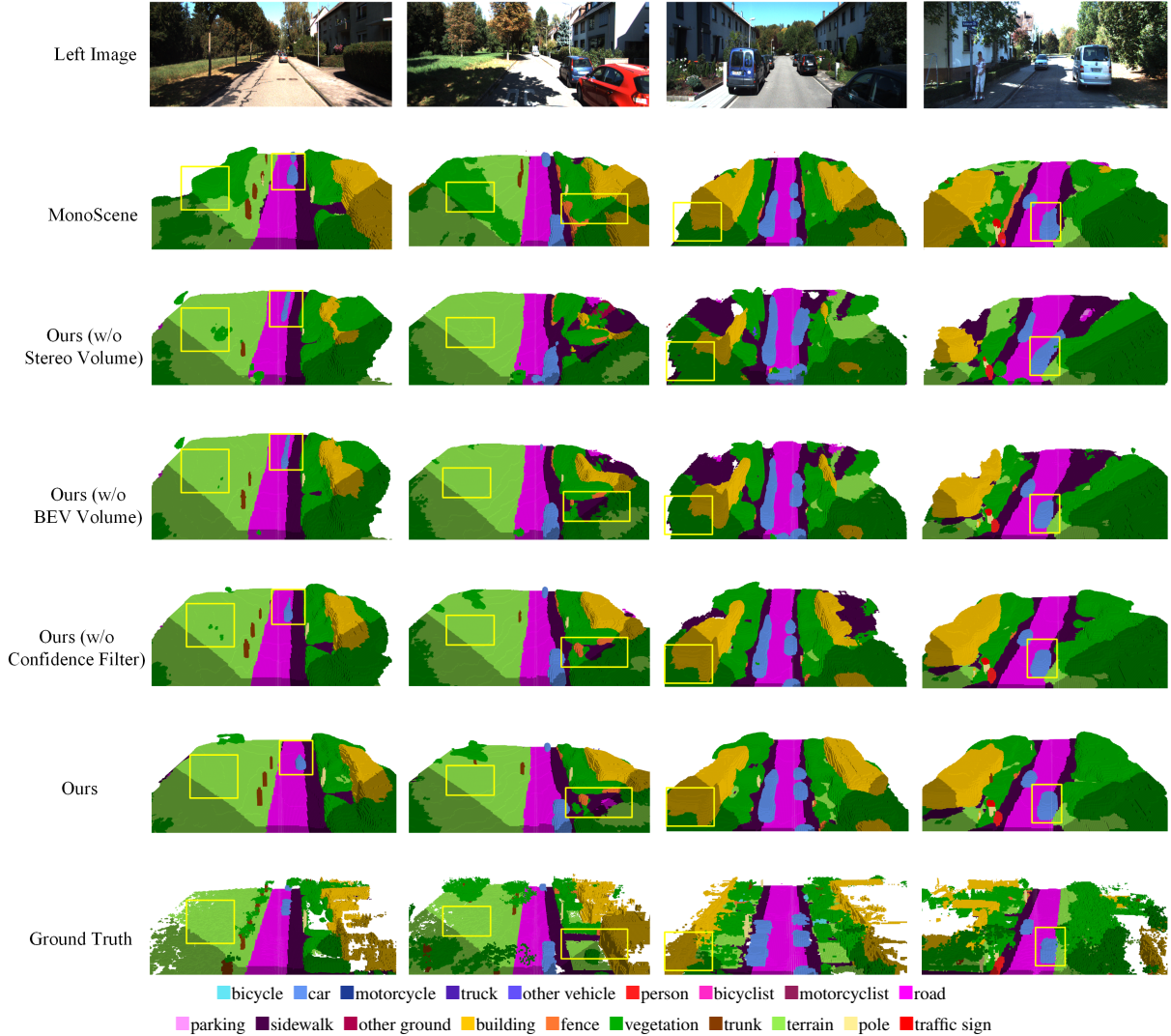


Figure 4: Qualitative results on the SemanticKITTI [1] validation set. The overlay shadow area at bottom of semantic prediction denotes unseen scenery out of camera’s field of view (FOV). StereoScene shows obvious advancement on small moving objects and proper hallucinations outside FOV.

compared to the geometric aspect, boosting IoU by 1.14 and mIoU by 1.58, respectively. For ‘w/o Confidence Filtering’, we remove the confidence filter and directly multiply the guidance attention matrix with the value vector, while both of the volumes are utilized and aggregated. The confidence filtering further improves the IoU (+0.66) and mIoU (+0.62) as expected.

Figure 4 visualizes the impact of the volumes. As the figure shows, the prediction results of scene semantics (e.g. sidewalk, column 2) and geometry (e.g. distant truck, column 2) are significantly improved with the introduction of BEV volume and stereo volume, respectively. It validates the effectiveness of our confidence filtering on retaining the high confidence regions for better aggregation (e.g. trunks, column1 and column 3).

5. Conclusion

In this work, we propose **StereoScene**, a BEV-assisted stereo matching 3D Semantic Scene Completion (SSC) framework that generates high-fidelity 3D scene understanding results without resorting to any external 3D geometric sensor inputs. We emphasize several appealing properties of our work: **1)** Without utilizing any pretrained 3D teacher network or explicit geometric inputs, we implicitly formulate a structured space through geometric constraint. **2)** A transformer-based *Mutual Interactive Aggregation Module* is delicately devised to take full advantage of complementary nature of BEV representation and Stereo Matching. **3)** Our model demonstrates great robustness at extreme conditions such as tiny objects recognition or scenery hallucination outside camera’s field of view.

References

- [1] Jens Behley, Martin Garbade, Andres Milioto, Jan Quenzel, Sven Behnke, Jürgen Gall, and Cyrill Stachniss. Towards 3d lidar-based semantic scene understanding of 3d point cloud sequences: The semantickitti dataset. *The International Journal of Robotics Research*, 40(8-9), 2021. 8, 12
- [2] Jens Behley, Martin Garbade, Andres Milioto, Jan Quenzel, Sven Behnke, Cyrill Stachniss, and Jurgen Gall. Semantickitti: A dataset for semantic scene understanding of lidar sequences. In *ICCV*, 2019. 2, 5
- [3] Yingjie Cai, Xuesong Chen, Chao Zhang, Kwan-Yee Lin, Xiaogang Wang, and Hongsheng Li. Semantic scene completion via integrating instances and scene in-the-loop. In *CVPR*, 2021. 2
- [4] Anh-Quan Cao and Raoul de Charette. Monoscene: Monocular 3d semantic scene completion. In *CVPR*, 2022. 2, 3, 5, 6, 11
- [5] Jia-Ren Chang and Yong-Sheng Chen. Pyramid stereo matching network. In *CVPR*, 2018. 3
- [6] Liang-Chieh Chen, George Papandreou, Iasonas Kokkinos, Kevin Murphy, and Alan L Yuille. Deeplab: Semantic image segmentation with deep convolutional nets, atrous convolution, and fully connected crfs. *IEEE transactions on pattern analysis and machine intelligence*, 40(4), 2017. 5
- [7] Liang-Chieh Chen, George Papandreou, Florian Schroff, and Hartwig Adam. Rethinking atrous convolution for semantic image segmentation. *arXiv preprint arXiv:1706.05587*, 2017. 13
- [8] Liang-Chieh Chen, Yukun Zhu, George Papandreou, Florian Schroff, and Hartwig Adam. Encoder-decoder with atrous separable convolution for semantic image segmentation. In *ECCV*, 2018. 13
- [9] Po-Heng Chen, Hsiao-Chien Yang, Kuan-Wen Chen, and Yong-Sheng Chen. Mvsnet++: Learning depth-based attention pyramid features for multi-view stereo. *IEEE Transactions on Image Processing*, 29, 2020. 2, 5
- [10] Xiaokang Chen, Kwan-Yee Lin, Chen Qian, Gang Zeng, and Hongsheng Li. 3d sketch-aware semantic scene completion via semi-supervised structure prior. In *CVPR*, 2020. 6
- [11] Ran Cheng, Christopher Agia, Yuan Ren, Xinhai Li, and Liu Bingbing. S3cnet: A sparse semantic scene completion network for lidar point clouds. In *Conference on Robot Learning*, 2021. 2
- [12] Ian Cherabier, Johannes L Schonberger, Martin R Oswald, Marc Pollefeys, and Andreas Geiger. Learning priors for semantic 3d reconstruction. In *ECCV*, 2018. 2
- [13] James Davis, Stephen R Marschner, Matt Garr, and Marc Levoy. Filling holes in complex surfaces using volumetric diffusion. In *3d data processing visualization and transmission*, 2002. 2
- [14] Lahav Lipson; Zachary Teed; Jia Deng. Raft-stereo: Multi-level recurrent field transforms for stereo matching. *3DV*, 2021. 3
- [15] Aloisio Dourado, Teofilo E De Campos, Hansung Kim, and Adrian Hilton. Edgenet: Semantic scene completion from a single rgb-d image. In *ICPR*, 2021. 2
- [16] George Fahim, Khalid Amin, and Sameh Zarif. Single-view 3d reconstruction: A survey of deep learning methods. *Computers & Graphics*, 94, 2021. 2
- [17] Martin Garbade, Yueh-Tung Chen, Johann Sawatzky, and Juergen Gall. Two stream 3d semantic scene completion. In *CVPRW*, 2019. 1, 2, 3
- [18] Andreas Geiger, Philip Lenz, and Raquel Urtasun. Are we ready for autonomous driving? the kitti vision benchmark suite. In *CVPR*, 2012. 6
- [19] Xiaoyang Guo, Kai Yang, Wukui Yang, Xiaogang Wang, and Hongsheng Li. Group-wise correlation stereo network. In *CVPR*, 2019. 2, 3, 11
- [20] Juyong Zhang Haofei Xu. Aaenet: Adaptive aggregation network for efficient stereo matching. *CVPR*, 2020. 3
- [21] Anthony Hu, Zak Murez, Nikhil Mohan, Sofia Dudas, Jeffrey Hawke, Vijay Badrinarayanan, Roberto Cipolla, and Alex Kendall. Fiery: future instance prediction in bird’s-eye view from surround monocular cameras. In *ICCV*, 2021. 3
- [22] Jie Hu, Li Shen, and Gang Sun. Squeeze-and-excitation networks. In *CVPR*, 2018. 5
- [23] Michael Kazhdan, Matthew Bolitho, and Hugues Hoppe. Poisson surface reconstruction. In *Eurographics symposium on Geometry processing*, volume 7, 2006. 2
- [24] Alex Kendall, Hayk Martirosyan, Saumitro Dasgupta, Peter Henry, Ryan Kennedy, Abraham Bachrach, and Adam Bry. End-to-end learning of geometry and context for deep stereo regression. In *ICCV*, 2017. 2, 3
- [25] Jie Li, Kai Han, Peng Wang, Yu Liu, and Xia Yuan. Anisotropic convolutional networks for 3d semantic scene completion. In *CVPR*, 2020. 2, 6
- [26] Jie Li, Yu Liu, Dong Gong, Qinfeng Shi, Xia Yuan, Chunxia Zhao, and Ian Reid. Rgb-d based dimensional decomposition residual network for 3d semantic scene completion. In *CVPR*, 2019. 2
- [27] Jiankun Li, Peisen Wang, Pengfei Xiong, Tao Cai, Ziwei Yan, Lei Yang, Jiangyu Liu, Haoqiang Fan, and Shuaicheng Liu. Practical stereo matching via cascaded recurrent network with adaptive correlation. *CVPR*, 2021. 3
- [28] Yiming Li, Zhiding Yu, Christopher Choy, Chaowei Xiao, Jose M Alvarez, Sanja Fidler, Chen Feng, and Anima Anandkumar. Voxformer: Sparse voxel transformer for camera-based 3d semantic scene completion. *arXiv preprint arXiv:2302.12251*, 2023. 2, 6
- [29] Zhiqi Li, Wenhao Wang, Hongyang Li, Enze Xie, Chonghao Sima, Tong Lu, Yu Qiao, and Jifeng Dai. Bevformer: Learning bird’s-eye-view representation from multi-camera images via spatiotemporal transformers. In *ECCV*, 2022. 2, 3
- [30] Ilya Loshchilov and Frank Hutter. Decoupled weight decay regularization. *arXiv preprint arXiv:1711.05101*, 2017. 6
- [31] Kaustubh Mani, Swapnil Daga, Shubhika Garg, Sai Shankar Narasimhan, Madhava Krishna, and Krishna Murthy Jatavallabhula. Monolayout: Amodal scene layout from a single image. In *WACV*, 2020. 3
- [32] Nikolaus Mayer, Eddy Ilg, Philip Häusser, Philipp Fischer, Daniel Cremers, Alexey Dosovitskiy, and Thomas Brox. A

- large dataset to train convolutional networks for disparity, optical flow, and scene flow estimation. *CVPR*, 2016. 3
- [33] Ruihang Miao, Weizhou Liu, Mingrui Chen, Zheng Gong, Weixin Xu, Chen Hu, and Shuchang Zhou. Occdepth: A depth-aware method for 3d semantic scene completion. *arXiv preprint arXiv:2302.13540*, 2023. 2
- [34] Richard A Newcombe, Shahram Izadi, Otmar Hilliges, David Molyneaux, David Kim, Andrew J Davison, Pushmeet Kohi, Jamie Shotton, Steve Hodges, and Andrew Fitzgibbon. Kinectfusion: Real-time dense surface mapping and tracking. In *IEEE international symposium on mixed and augmented reality*, 2011. 2
- [35] Mong H Ng, Kaahan Radia, Jianfei Chen, Dequan Wang, Ionel Gog, and Joseph E Gonzalez. Bev-seg: Bird’s eye view semantic segmentation using geometry and semantic point cloud. *arXiv preprint arXiv:2006.11436*, 2020. 3
- [36] James Okae, Bohan Li, Juan Du, and Yueming Hu. Robust scale-aware stereo matching network. *IEEE Transactions on Artificial Intelligence*, 2021. 3
- [37] Bowen Pan, Jiankai Sun, Ho Yin Tiga Leung, Alex Andonian, and Bolei Zhou. Cross-view semantic segmentation for sensing surroundings. *IEEE Robotics and Automation Letters*, 5(3), 2020. 3
- [38] Jiahao Pang, Wenxiu Sun, Jimmy SJ. Ren, Chengxi Yang, and Qiong Yan. Cascade residual learning: A two-stage convolutional neural network for stereo matching. *ICCVW*, 2017. 3
- [39] Adam Paszke, Sam Gross, Francisco Massa, Adam Lerer, James Bradbury, Gregory Chanan, Trevor Killeen, Zeming Lin, Natalia Gimelshein, Luca Antiga, et al. Pytorch: An imperative style, high-performance deep learning library. *NeurIPS*, 32, 2019. 6
- [40] Jonah Philion and Sanja Fidler. Lift, splat, shoot: Encoding images from arbitrary camera rigs by implicitly unprojecting to 3d. In *ECCV*, 2020. 3, 4, 5, 11
- [41] Matteo Poggi, Fabio Tosi, Konstantinos Batsos, Philippos Mordohai, and Stefano Mattoccia. On the synergies between machine learning and binocular stereo for depth estimation from images: A survey. *IEEE Transactions on Pattern Analysis and Machine Intelligence*, 2022. 2
- [42] Cody Reading, Ali Harakeh, Julia Chae, and Steven L Waslander. Categorical depth distribution network for monocular 3d object detection. In *CVPR*, 2021. 3
- [43] Christoph B Rist, David Emmerichs, MarkusENZweiler, and Dariu M Gavrila. Semantic scene completion using local deep implicit functions on lidar data. *IEEE transactions on pattern analysis and machine intelligence*, 44(10), 2021. 2
- [44] Lawrence G Roberts. *Machine perception of three-dimensional solids*. PhD thesis, Massachusetts Institute of Technology, 1963. 1
- [45] Thomas Roddick and Roberto Cipolla. Predicting semantic map representations from images using pyramid occupancy networks. In *CVPR*, 2020. 3
- [46] Luis Roldao, Raoul de Charette, and Anne Verroust-Blondet. Lmscnet: Lightweight multiscale 3d semantic completion. In *3DV*, 2020. 1, 2, 3, 6
- [47] Luis Roldao, Raoul De Charette, and Anne Verroust-Blondet. 3d semantic scene completion: A survey. *International Journal of Computer Vision*, 130(8), 2022. 1
- [48] Zhelun Shen, Yuchao Dai, and Zhibo Rao. Cfnets: Cascade and fused cost volume for robust stereo matching. In *CVPR*, 2021. 11
- [49] Nathan Silberman, Derek Hoiem, Pushmeet Kohli, and Rob Fergus. Indoor segmentation and support inference from rgb-d images. *ECCV*, 2012. 2
- [50] Shuran Song, Fisher Yu, Andy Zeng, Angel X Chang, Manolis Savva, and Thomas Funkhouser. Semantic scene completion from a single depth image. In *CVPR*, 2017. 2, 6
- [51] Olga Sorkine and Daniel Cohen-Or. Least-squares meshes. In *Proceedings Shape Modeling Applications*, 2004. 2
- [52] Julian Straub, Thomas Whelan, Lingni Ma, Yufan Chen, Erik Wijmans, Simon Green, Jakob J Engel, Raul Mur-Artal, Carl Ren, Shobhit Verma, et al. The replica dataset: A digital replica of indoor spaces. *arXiv preprint arXiv:1906.05797*, 2019. 2
- [53] Mingxing Tan and Quoc Le. Efficientnet: Rethinking model scaling for convolutional neural networks. In *ICML*, 2019. 3
- [54] Vladimir Tankovich, Christian Häne, Yinda Zhang, Adarsh Kowdle, Sean Fanello, and Sofien Bouaziz. Hitnet: Hierarchical iterative tile refinement network for real-time stereo matching. *CVPR*, 2021. 3
- [55] Xiaolong Wang, Ross Girshick, Abhinav Gupta, and Kaiming He. Non-local neural networks. In *CVPR*, 2018. 4
- [56] Xiaofeng Wang, Zheng Zhu, Guan Huang, Fangbo Qin, Yun Ye, Yijia He, Xu Chi, and Xingang Wang. Mvster: epipolar transformer for efficient multi-view stereo. In *ECCV*, 2022. 4
- [57] Yue Wang, Vitor Campagnolo Guizilini, Tianyuan Zhang, Yilun Wang, Hang Zhao, and Justin Solomon. Detr3d: 3d object detection from multi-view images via 3d-to-2d queries. In *Conference on Robot Learning*, 2022. 3
- [58] Shun-Cheng Wu, Keisuke Tateno, Nassir Navab, and Federico Tombari. Scfusion: Real-time incremental scene reconstruction with semantic completion. In *3DV*, 2020. 1, 2, 3
- [59] Xu Yan, Jiantao Gao, Jie Li, Ruimao Zhang, Zhen Li, Rui Huang, and Shuguang Cui. Sparse single sweep lidar point cloud segmentation via learning contextual shape priors from scene completion. In *AAAI*, volume 35, 2021. 2, 6
- [60] Yurong You, Yan Wang, Wei-Lun Chao, Divyansh Garg, Geoff Pleiss, Bharath Hariharan, Mark Campbell, and Kilian Q Weinberger. Pseudo-lidar++: Accurate depth for 3d object detection in autonomous driving. *arXiv preprint arXiv:1906.06310*, 2019. 4
- [61] Jiahui Zhang, Hao Zhao, Anbang Yao, Yurong Chen, Li Zhang, and Hongen Liao. Efficient semantic scene completion network with spatial group convolution. In *ECCV*, 2018. 2
- [62] Min Zhong and Gang Zeng. Semantic point completion network for 3d semantic scene completion. In *ECAI*. IOS Press, 2020. 2

Supplementary Material of BEV-Assisted Stereo Matching Empowers 3D Semantic Scene Completion

A. More Visualization Results

Below we provide qualitative comparisons on SemanticKITTI validation set and show visualization examples in Figure 5. Compared to MonoScene [4], our **StereoScene** generates more precise predictions (e.g. truck, example 1; car, example 3) and more complete scenes with proper hallucinations (e.g. example 2).

Specifically, in example 1, MonoScene predicts wrong shape for truck instance prediction (see yellow circle). In example 2, compared to MonoScene, our method successfully hallucinates a more complete and reasonable scene outside the camera FOV. Moreover, the semantics generated by StereoScene is consistent with the holistic scenes in most regions. In example 3, StereoScene precisely capture the semantic and geometry of car while MonoScene faces challenges in correct recognition.

B. Implementation Details on Dual Volume Construction

In this section, we describe implementation details for our dual volume construction. The *Stereo Representation Construction* module targets to match 2D extracted features and outputs a structural 3D representation, regularized depth volume. The *BEV Representation Construction* module constructs a 3D latent volume coupled with context features from 2D image features.

More Details on Stereo Representation Construction. As mentioned in Sec. 3.2 of the main paper, we construct stereo geometric volume from the left and right image features. For the purpose of being aware of distinct camera inputs, we also feed the camera parameters P_i (concatenated intrinsic and extrinsic) to a **Parameter Encoder** as shown in Figure 6. Formally,

$$P_e = \sigma(\text{Conv}(\text{Reshape}(\text{FC}(P_i)))) \quad (12)$$

where Conv and FC are convolutions and fully-connected layers, whereas σ and Reshape represent sigmoid function and reshape operation, respectively. The encoded camera parameters P_e are multiplied with the extracted features to generate the camera-aware features.

The left and right camera-aware unary features are correlated to form the group-wise disparity volume, which is then converted to depth volume. To regularize the depth volume,

Name	Layer Properties	Dim	Input
Conv1	$3 \times 3 \times 3, 2, 1$	32/64	Input Volume
Conv2	$3 \times 3 \times 3, 1, 1$	64/64	Conv1
Conv3	$3 \times 3 \times 3, 2, 1$	64/128	Conv2
Conv4	$3 \times 3 \times 3, 1, 1$	128/128	Conv3
Deconv5	$3 \times 3 \times 3, 2, 1$	128/64	Conv4
Conv6	$1 \times 1 \times 1, 1, 0$	64/64	Conv2
Shortcut	Addition & ReLU	64/64	Deconv5, Conv6
Deconv7	$3 \times 3 \times 3, 2, 1$	64/32	Shortcut
Conv8	$1 \times 1 \times 1, 1, 0$	32/32	Input Volume
Output Volume	Addition & ReLU	32/32	Deconv7, Conv8

Table 6: Structure details of the 3D hourglass. The "Layer Properties" indicates kernel size, stride and padding, respectively.

we adopt 3D CNNs with hourglass (encoder-decoder) structures to process it [19, 48]. As shown in Figure 6, we first feed the depth volume to four $3 \times 3 \times 3$ convolutions with stride 1, the last two of which are implemented with residual connection.

With the depth volume, we employ three stacked 3D hourglasses to further aggregate the volumetric information. The structure details of the 3D hourglass are shown in Table 6, where two residual connections are adopted to aggregate contexts from different semantic levels. In each 3D hourglass, the input volume is first downsampled and then upsampled with deconvolution, thus aggregating information along the spatial and depth dimensions. Finally, two $3 \times 3 \times 3$ convolutions are used to generate the regularized depth volume with dimension of $\mathbb{R}^{1 \times D \times H \times W}$.

More Details on BEV Representation Construction. As mentioned in Sec. 3.2 of the main paper, we construct BEV context features and BEV latent volume as BEV representations [40]. In our implementation, we adopt left image features and camera parameters as inputs.

As shown in Figure 7, two branches are employed in parallel, where the upper branch is dedicated to generating contextual features while the lower branch is dedicated to generating latent volume. For both branches, we use camera parameter encoder similar to Equation 12 for camera-awareness. In the upper branch, a 3×3 convolu-

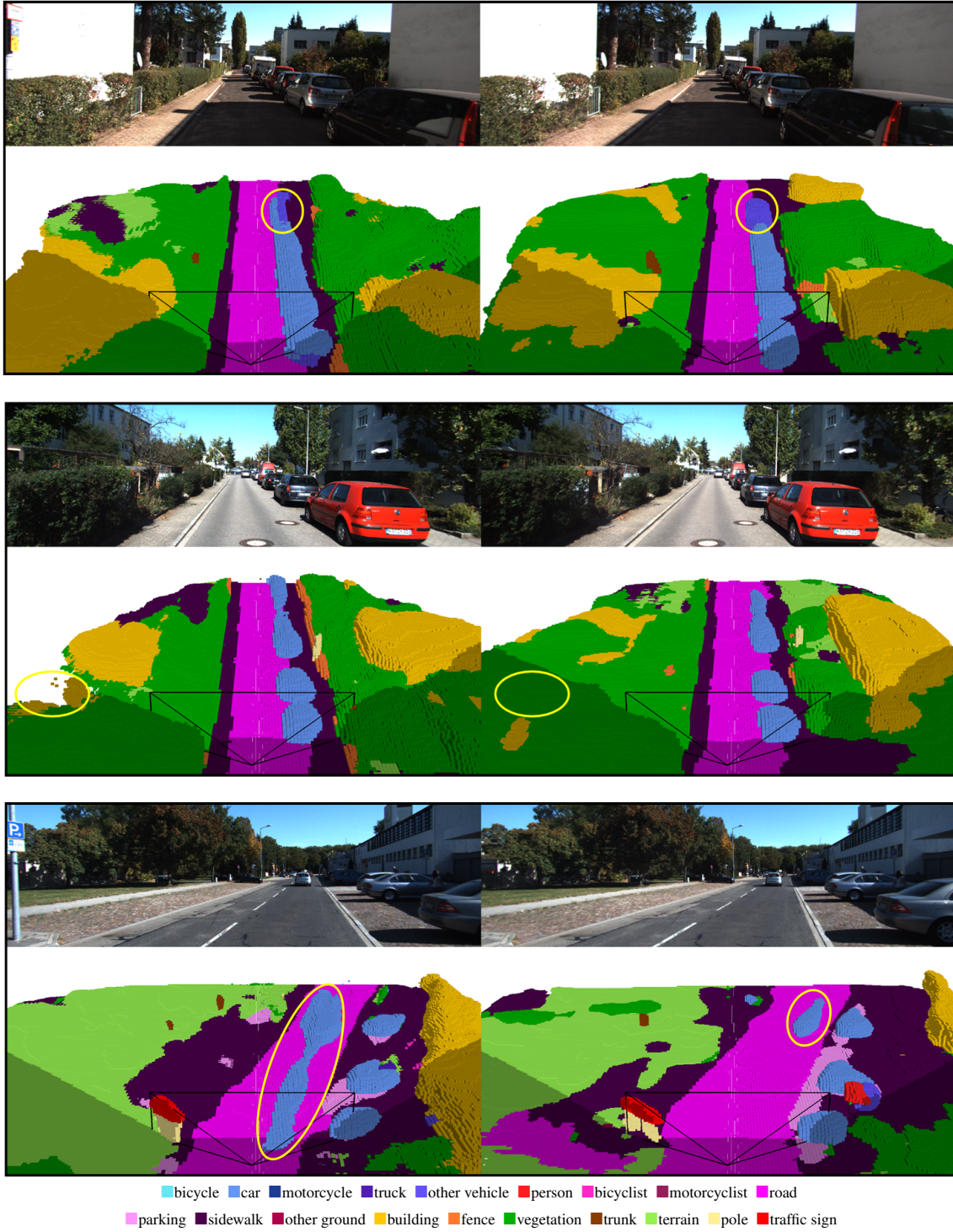


Figure 5: More visualization results on the SemanticKITTI [1] validation set. From top to below demonstrate 3 cases. For each one, the first row illustrates stereo input images while the second row depicts comparison results of MonoScene and StereoScene.

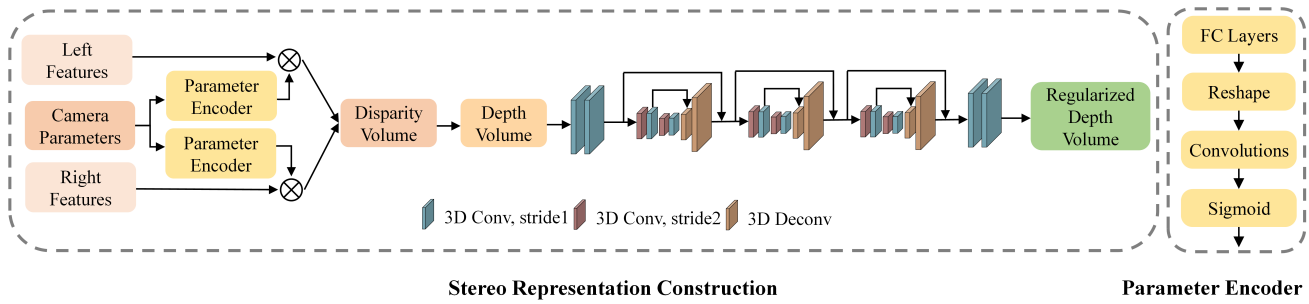


Figure 6: Implementation details of the stereo representation construction. The left and right features are encoded with camera parameters before forming the disparity volume.

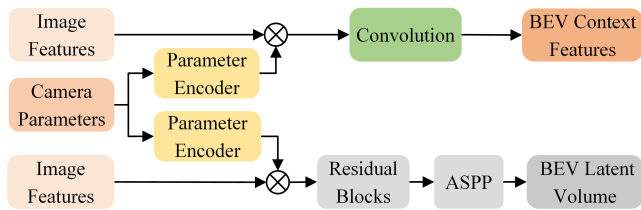


Figure 7: Implementation details of the BEV representation construction. We employ two branches in parallel to generate the BEV context features and BEV latent volume.

tion is adopted to generate the context features. In the lower branch, we adopt two stacked residual blocks and an ASPP [7, 8] module to refine the depth distribution of the latent volume. The ASPP module is used to expand the receptive field in depth perception process, which contains four atrous convolutions with dilation rates of 1, 6, 12, 18, respectively.